Int J Coal Sci Technol (2014) 1(1):46–55
DOI 10.1007/s40789-014-0003-8

Research on the maceral characteristics of Shenhua coal and efficient and directional direct coal liquefaction technology

Geping Shu · Yuzhuo Zhang

Received: 1 December 2013 / Revised: 10 January 2014 / Accepted: 13 January 2014 / Published online: 12 September 2014

Abstract In this research, molecular structure models were developed respectively for Shenhua coal vitrinite concentrates (SDV) and inertinite concentrates (SDI), on the basis of information on constitutional unit of Shenhau coal and elemental analysis results obtained from ^{13}C-NMR analysis characterization, FTIR analysis characterization, X-ray diffraction XRD and XPS analysis characterization. It can be observed from characterization data and molecular structure models that the structure of SDV and SDI is dominated by aromatic hydrocarbon, with aromaticity of SDI higher than that of SDV; SDV mainly consists of small molecule basic structure unit, while SDI is largely made from macromolecular structure unit. Based on bond-level parameters of the molecular model, the research found through the autoclave experiment that vitrinite liquefaction process goes under thermodynamics control and inertinite liquefaction process under dynamics control. The research developed an efficient directional direct coal liquefaction technology based on the maceral characteristics of Shenhua coal, which can effectively improve oil yield and lower gas yield.

Keywords Liquefaction · Maceral · Molecular model · Shenhua coal · Directional direct coal liquefaction

1 Introduction

Generally, direct coal liquefaction process chooses coal as the single feedstock and aims to produce distillable liquids. This process lends itself to coal with low level of inertinite if maximum liquids production is a prerequisite for the selection of process route and appropriate reaction conditions in a reaction system. China Coal Research Institute conducted a study on properties of Chinese coal for direct liquefaction (Shu and Xu 1997) and selected 15 types of coals suitable for direct liquefaction, with inertinite content of the top 10 all less than 7 %. However, Shenhua coal maceral has higher inertinite content level, with some even more than 60 %, than that of any other coals in China or even in the world. Therefore, it is necessary to study the maceral structures of Shenhua coal and consequent differences of their liquefaction performance and then develop an efficient directional direct liquefaction technology based on the characteristics of Shenhua coal maceral.

G. Shu (✉) · Y. Zhang
Shenhua Group Co., Ltd., Beijing 100011, China
e-mail: shugeping@csclc.com

2 Experimental

2.1 Sample preparation

Shenhua coal samples (SDR) were collected from Shangwan coal mine, Shendong, Inner Mongolia. The raw coal was prepared by hand and a drifting process to obtain vitrinite concentrates (SDV) and inertinite concentrates (SDI). Industrial analysis and elemental analysis of Shenhua coal, vitrinite concentrates and inertinite concentrates are shown in Table 1, as well as petrographical analysis in Table 2.

Table 1 Proximate and ultimate analysis of coal samples

Sample	Proximate analysis (w %)				Ultimate analysis (W_{daf} %)			
	M_{ad}	A_d	V_{daf}	C	H	N	S	O*
SDR	8.45	17.03	38.19	79.29	4.30	0.86	0.47	15.08
SDI	10.96	5.27	30.59	82.12	3.79	0.86	0.40	12.83
SDV	10.60	2.27	40.47	80.55	4.72	1.06	0.41	13.26

* By differences, *SDR* Shendong coal, *SDV* vitrinite concentrate obtained from Shendong coal, *SDI* inertinite concentrate obtained from Shendong coal

Table 2 Petrographical analysis %

Sample	Vitrinite	Inertinite	Exinite	R_{max}
SDV	82.2	16.4	0.7	
SDR	42.5	52.3	0.8	0.519
SDI	17.8	80.1	0.5	

2.2 ^{13}C-NMR analysis characterization

The research adopted an NMR AVANCE400 superconducting spectrometer produced by Bruker company, with a solid double resonance probe, and a 4 mm ZrO_2 rotor; magic-angle speed was set at 8,000 Hz, resonance frequency 100.13 MHz, the sampling time 0.05 s, pulse wide 4 μs, cyclic delay time 5 s, and 7,000 scan times. The cross polarization (CP) technology was applied as well.

2.3 FTIR analysis characterization

Instrument type: US Nicolet 6700 FT-IR; test conditions: wavelength range: 4,000–400 cm^{-1}, accuracy: wave number ≤0.1/cm; transmittance ≤0.1, resolution: 4 cm^{-1}, number of scans: 32 times.

2.4 X-ray diffraction XRD

Instrument type: D/MAX 2550 VB/PC, manufacturer: Japan RIGAKU. Test method: wavelength: 1.54056 angstrom; copper target: 40 kV, 100 mA; scanning speed: 12 degrees/min, step: 0.02 degree.

2.5 XPS analysis characterization

XPS measurement is conducted with ESCALAB250 X-ray photoelectron spectroscopy. Use AlKa anode, and the power is 200 W. The full scan penetration power is 150 eV, step length 0.5 eV; narrow scan penetration power 60 eV, step 0.05 eV. Basic vacuum is 10^{-7} Pa. Take C1s (284.6 eV) as the calibration standard. The ordinate in the XPS spectra represents electronic counting, while the abscissa shows the electron binding energy (Binding Energy, B.E.).

2.6 Experiment of coal liquefaction reaction in autoclave

The coal liquefaction experiment used 0.5 L stirred autoclave, and the standard experimental conditions are as follows: coal input is 28 g (dry coal), initial hydrogen pressure is 10.0 MPa, the mass ratio of solvent to the coal is 1.5:1, the catalyst is Fe_2O_3, the additive amount of Fe is 3 % of the mass of dry coal, sulfur is the co-catalyst, n(S)/n(Fe) = 2. Heating rate is 8 °C/min till the set reaction temperature is reached. After the reaction, the temperature in the autoclave drops to 200 °C within 20 min. Products out of the autoclave include two parts: gaseous phase products, the component of which is analyzed with gas chromatography, and liquid–solid mixture which gets Soxhlet extraction separation successively with n-hexane and then tetrahydrofuran, finding that n-hexane soluble substance is oil, n-hexane insoluble and THF-soluble substances consist of pre-asphaltene and asphaltene (for short, PPA), THF-insoluble substances contains unreacted coal and ash. Analytical extraction procedures can be seen in literature (Shu et al. 2003).

2.7 Bench-scale unit for continuous direct coal liquefaction experiment

The continuous direct coal liquefaction experiment used a small continuous bench-sacle unit (BSU) with daily handling capacity of 120 kg of dry coal. Ordinary process unit has a reaction system of two bubbling bed reactors in series, while the reaction system of Shenhua unit has two reactors in series equipped with a circulating pump at the bottom and a gas–liquid separator on the top (Shu 2009).

3 Results and discussions

3.1 Macromolecular structure model of SDV and SDI

^{13}C-CP/MAS NMR analytical characterization, X-ray diffraction, FTIR analytical characterization, X-ray diffraction XRD, and XPS analytical characterization were applied to the sample.

^{13}C-CP/MAS NMR peak-fitting spectra of Shendong Shangwan SDV and SDI are illustrated respectively in Figs. 1 and 2, with the structure parameters shown in Table 3.

It can be observed from Figs. 1 and 2, ^{13}C spectra of Shendong coal obviously has two peaks, one chemical shift located at aliphatic carbon of 0–60 ppm and the other at aromatic area of 90–165 ppm. However, these two samples at the aromatic area are obviously larger than those at the

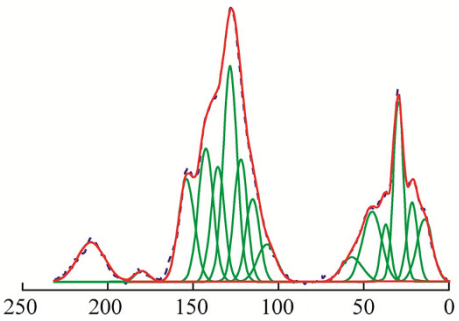

Fig. 1 ^{13}C-CP/MAS NMR spectra of Shenhua coal vitrinite

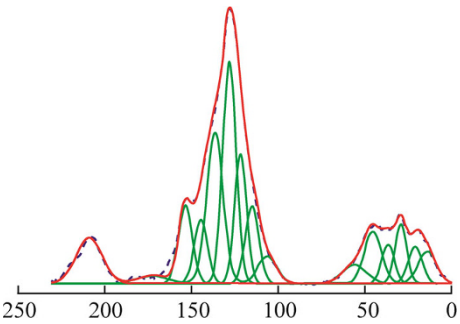

Fig. 2 ^{13}C-CP/MAS NMR spectra of Shenhua coal inertinite

aliphatic area, and the aliphatic area of inertinite group is obviously smaller than that of vitrinite group.

Aromaticity ($f_a^{'}$) is an important parameter of coal structure. As can be seen from Table 5, aromaticity of inertinite is obviously higher than that of vitrinite. There is a big difference between inertinite at 67.47 % and vitrinit at 61.47 %. The comparison concludes that the biggest difference of aromatic carbon is caused by f_a^{C} (carbonyl), f_a^{S} (alkylated aromatic) and f_a^{B} (aromatic bridgehead). The vitrinite has more alkylated aromatic, while the inertinite has more aromatic bridgehead.

The ratio of aromatic bridgehead carbons to total ring carbons serves as an important parameter to research the macromolecular structure of coal, which can be used to calculate the size of aromatic clusters in coal structures. The types and number of aromatic structure units in the molecular structure of coal can be basically determined on the basis of this parameter. The hydrogen aromaticity is used to represent the concentration of aromatic hydrogen in coal structure, with its formula of calculation as below: $H_a = (C/H)_{atom} \times f_a^H$. The values of X_b and H_a of these two samples are shown in Table 4.

As can be seen from the X_b values in Table 4, the ratios of aromatic bridgehead carbons to total ring carbons for SDV and SDI are very different. This indicates that these two coal samples have a big difference in macromolecular structure. The ratio of inertinite group is 0.307, much more

Table 4 Coal-related structure parameters

Sample	X_b	H_a
SDV	0.154	2.29
SDI	0.307	2.67

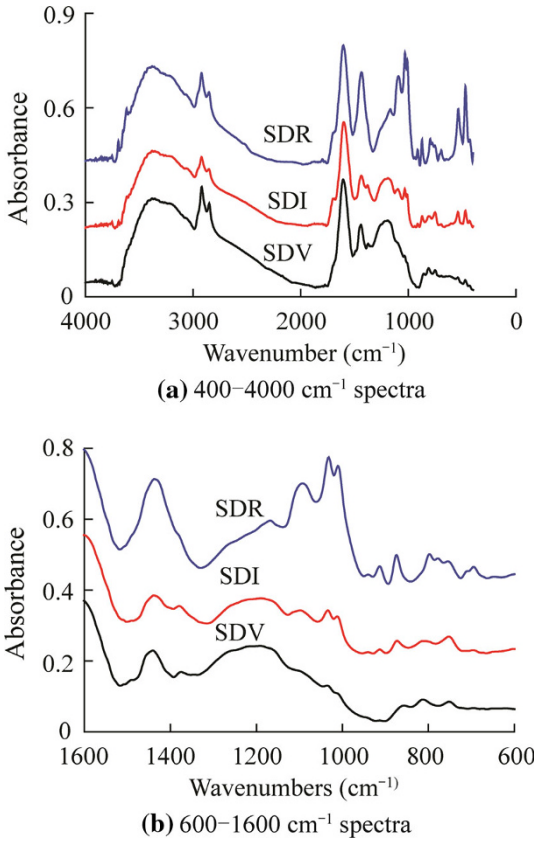

Fig. 3 FTIR spectra of SDV and SD

Table 3 Structure parameters of samples %

Sample	f_a	f_a^C	$f_a^{'}$	f_a^N	f_a^H	f_a^P	f_a^S	f_a^B	f_{al}	f_{al}^*	f_{al}^H	f_{al}^O
SDV	67.96	6.49	61.47	27.39	34.09	8.77	10.43	8.18	32.03	16.76	12.60	2.68
SDI	76.71	9.24	67.47	28.5	38.97	7.15	5.49	15.87	23.29	7.05	13.38	2.86

f_a Total aromatic carbon, f_{al} total aliphatic carbon, f_a^C carbonyl δ(chemical shift) >165 $\times$ 10^{-6}, $f_a^{'}$ in an aromatic ring, f_a^H protonated and aromatic, f_a^N onprotonated and aromatic, f_a^P phenolic or phenolic ether, f_a^S alkylated aromatic, f_a^B aromatic bridgehead, f_{al}^* CH_3 or nonprotonated, f_{al}^H (CH or CH_2), f_{al}^O bonded to oxygen

than vitrinite group (0.154). With respect to H_a, the inertinite group is higher, indicating that its coal structure has more aromatic ring structures. Such result remains consistent with the result of X_b.

The Fig. 3 illustrates the FTIR spectroscopic analysis spectra of SDV concentrates and SDI concentrates.

The ratio of aliphatic hydrogen (H_{al}) and aromatic hydrogen (H_{ar}) in the coal serves as an important parameter to research the coal structure, and in general the ratio of 2,800–3,000 cm^{-1} aliphatic–CH stretching vibration absorption area to 700–900 cm^{-1} aromatic–CH bending vibration absorption area represents the proportion of aliphatic hydrogen to aromatic hydrogen. Peak-fitting information was obtained through peak-fitting analysis of the infrared spectra of two coal samples, and the relevant structure parameter is calculated with the information. See it in Table 5. As can be seen from Table 5, the value of H_{al}/H_{ar} of SDV is 2.18, much higher than that of SDI (1.36), which indicates the structure has more aliphatic structure; it can be seen through $A_{2,800–3,000}/A_{1,600}$ that SDI is much smaller than SDV, indicating there are more aromatic frame in its structures; the ratio of $\nu(CH_2)/\nu(CH_3)$ leads to the conclusion that vitrinite and inertinite have more stretching vibration CH_2. These all provide information for establishing macromolecular structure of coal.

Table 5 Relevant parameters of three samples of SDR, SDV and SDI

Sample	Calculation	SDV	SDI
H_{al}/H_{ar}	$A_{2,800–3,000}/A_{700–900}$	2.18	1.36
Aliphatics/aromatics	$A_{2,800–3,000}/A_{1,600}$	0.36	0.23
$\nu(CH_2)/\nu(CH_3)$	$A_{2,926+2,854}/A_{2,956+2,875}$	3.83	3.62

Table 6 XPS C1s analysis of coal sample

B.E./eV	Carbon form	Content (W_{mol} %)	
		SDV	SDI
284.8	C–C,C–H	73.90	68.50
286.2	C–O	15.85	17.57
287.5	C=O	2.58	3.99
289.6	COO–	7.67	9.94

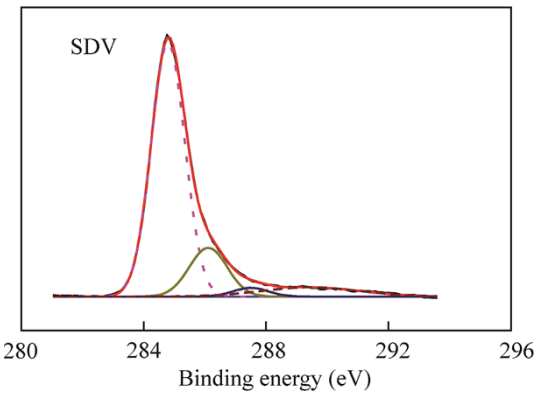

Fig. 4 C1s X-ray photoelectron spectroscopy of SDV

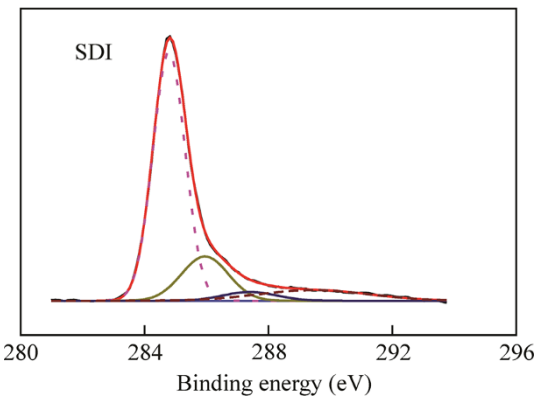

Fig. 5 C1s X-ray photoelectron spectroscopy of SDI

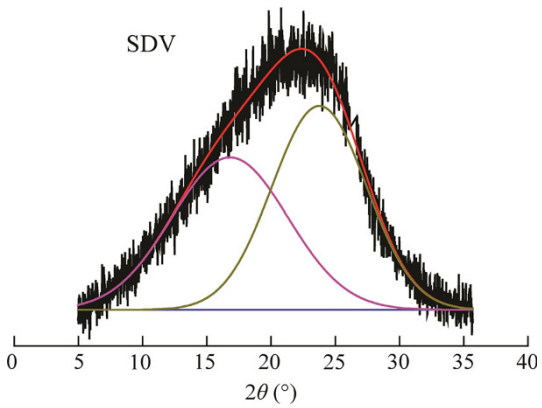

Fig. 6 5–40 XRD and peak-fitting graph of SDV sample

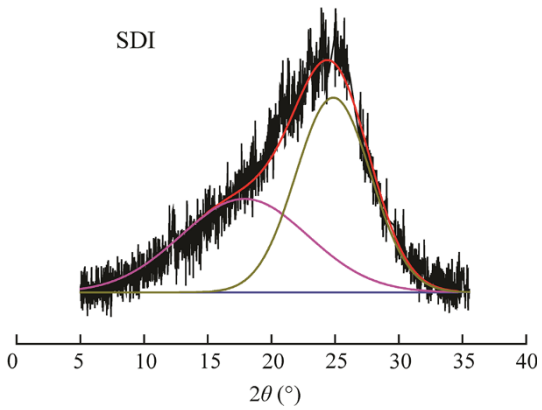

Fig. 7 5–40 XRD and peak-fitting graph of SDI sample

Table 7 XRD structure parameters of SDV and SDI

Samples	$2\theta_{002}$ (°)	β_{002}	$2\theta_{\gamma}$ (°)	θ_{100} (°)	d_{002} (Å)	d_{γ} (°)	L_c (°)	L_a (°)	N_c	f_a
SDV	23.77	8.645	16.82, 10.64	42.65,10.77	3.74	5.27	9.81	16.19	2.62	0.52
SDI-1	24.86	6.924	17.88, 11.80	43.72, 9.38	3.58	4.96	12.27	18.66	3.43	0.55

d_{002} (°) Inter aromatic layer distance, nm; L_c diameter of the aromatic clusters perpendicular to the plane of the sheet, nm; L_a diameter of aromatic sheet carbons of side chains from diamond's curve(10) band, nm; N_c average number of aromatic sheets associated in a stacked cluster; $f_a = C_A/C_{total} = A_{002}/(A_{002} + A\gamma)$

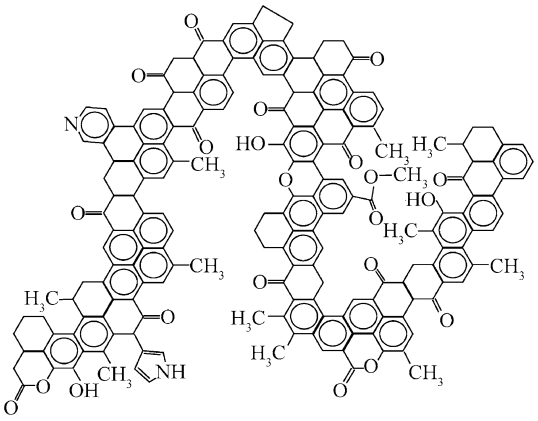

Fig. 8 Modified structural model of inertinite

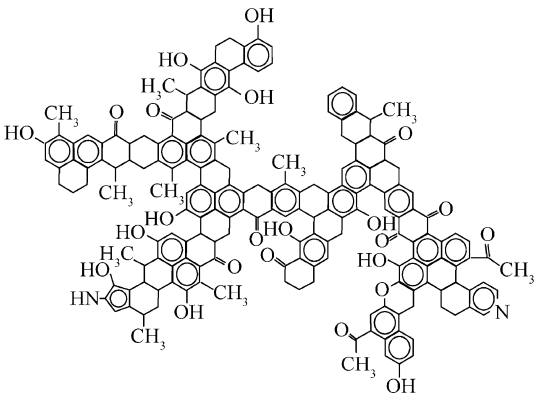

Fig. 9 Modified structural model of vitrinite

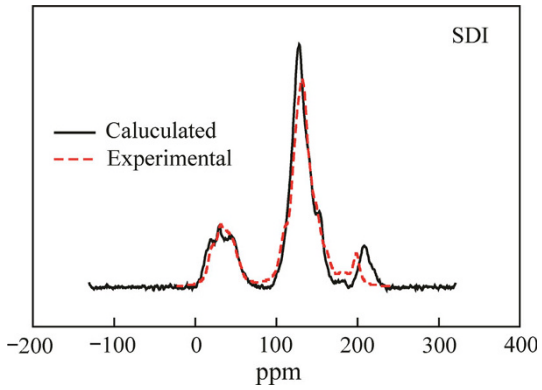

Fig. 10 The comparison between calculated values and experimental values of inertinite ^{13}C-NMR

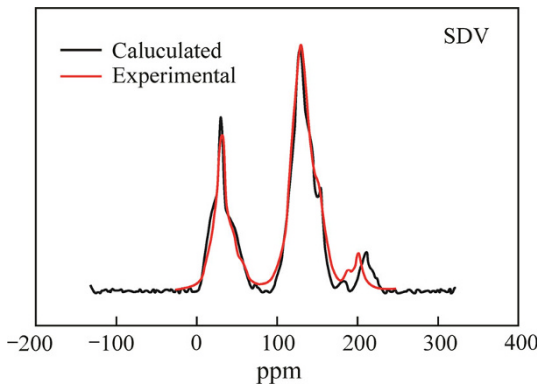

Fig. 11 The comparison between calculated values and experimental values of vitrinite ^{13}C-NMR

The XPS C1s spectra and peak-fitting graphs of SDV and SDI samples are illustrated respectively in Figs. 4 and 5. As can be seen from the figures, carbon has four forms in the coal surface structure. The peak 284.6 eV is attributable to aromatic unit and alkyl-substituted aromatic carbon (C–C, C–H); the peak 286.3 eV is attributable to phenolic carbon or ether carbon (C–O); the peak 287.5 eV is attributable to carbonyl (C=O) and the peak 289.0 eV belongs to carboxyl (COO–). Table 6 shows the XPS C1s results and distribution of samples.

As can be seen from Table 6, the surface structure of SDI has less content of C–C, C–H, indicating less alkyl side chains. A part of alkyl side chains are transformed into phenolic hydroxyl group and ether linkage under the effect of fusainization, which leads to the relatively higher mass fraction of C–O in SDI.

The 5–40 XDR peak-fitting graphs for SDV and SDI samples are illustrated respectively in Figs. 6 and 7. XDR structure parameter is shown in Table 7.

Using the ACD/CNMR predictor combined with data in Table 1, the research established SDV and SDI structure models respectively, as illustrated in Figs. 8 and 9. A ^{13}C

Table 8 SDV bond order distribution

Bond name	Bond order	Bond name	Bond order	Bond name	Bond order
O192–C209	0.860	C137–C136	0.991	C74–C82	1.272
C46–O44	0.885	C136–C133	0.991	C97–C96	1.274
C107–C110	0.929	C28–C31	0.991	C15–C14	1.276
O205–C180	0.933	C209–C57	0.992	C149–C147	1.277
C47–C45	0.938	C58–C57	0.992	C146–C140	1.278
C106–C187	0.938	C67–C66	0.994	C33–C32	1.282
C28–C26	0.940	C135–C134	0.995	C62–C61	1.286
C114–C110	0.943	C211–C172	0.995	C119–C118	1.288
C123–C120	0.944	C168–C167	0.995	C144–C143	1.289
C57–C54	0.944	C43–C14	0.996	C39–C37	1.291
C210–C108	0.946	C162–C157	0.996	C64–C62	1.293
C213–C186	0.947	C102–C100	0.997	C180–C179	1.293
C115–C114	0.948	C20–O190	0.997	C160–C159	1.295
C59–C55	0.948	C36–C35	1.000	C175–C111	1.296
C122–C121	0.949	C120–C25	1.000	C60–C63	1.299
C200–C199	0.950	C9–C191	1.000	C131–C130	1.300
C102–C195	0.950	O44–C15	1.001	C88–C85	1.302
C167–C164	0.950	C216–C106	1.001	C68–C67	1.302
C27–C26	0.951	O152–C149	1.002	C85–C84	1.303
C56–C55	0.954	C60–C59	1.003	C182–C180	1.304
C187–C186	0.954	C203–C129	1.004	C181–C68	1.304
C78–C115	0.957	C132–C218	1.005	C172–C171	1.310
C106–C98	0.957	C191–C8	1.008	C132–C119	1.314
C45–C46	0.958	C4–C3	1.009	C58–C64	1.314
C92–C89	0.960	O188–C127	1.012	C35–C34	1.314
C200–C71	0.962	C50–C47	1.019	C60–C58	1.316
C163–C162	0.963	O189–C85	1.021	C149–C148	1.316
C215–C210	0.963	O192–C10	1.027	C179–C67	1.317
C55–C54	0.963	O185–C63	1.028	C35–C40	1.318
O190–C41	0.964	O69–C64	1.028	C177–C112	1.322
C153–O152	0.965	C104–C23	1.030	C84–C83	1.323
C92–C91	0.965	O202–C175	1.033	C182–C181	1.325
C84–C73	0.967	O206–C130	1.035	C14–C13	1.327
C198–C102	0.967	O183–C24	1.037	C170–C169	1.330
C91–C90	0.967	C22–C27	1.043	C112–C111	1.332
C215–C177	0.967	O166–C148	1.054	C38–C37	1.332
C165–C164	0.968	C62–C68	1.054	C88–C87	1.334
C217–C215	0.968	C13–C56	1.059	C133–C131	1.335
C73–C74	0.969	O184–C179	1.062	C87–C86	1.335
C199–C210	0.969	O201–C182	1.063	C15–C8	1.336
C111–C109	0.970	O105–C16	1.072	C61–C63	1.337
C204–C198	0.970	C79–C119	1.077	C171–C169	1.338
C11–C54	0.970	C6–C5	1.089	C130–C118	1.343
C122–C120	0.971	C129–N128	1.117	C133–C132	1.345
C126–C124	0.971	C140–C139	1.149	C176–C175	1.345
C200–C193	0.973	C135–C138	1.160	C23–C22	1.351
C48–C46	0.974	C141–C137	1.160	C178–C177	1.355
C108–C107	0.974	N128–C127	1.182	C40–C38	1.357
C77–C107	0.975	C7–C5	1.188	C147–C146	1.358
C45–C43	0.975	C157–C155	1.192	C25–C24	1.359
C198–C197	0.975	C19–C22	1.193	C11–C10	1.369
C195–C194	0.975	C6–C2	1.194	C29–C33	1.373
C72–C71	0.975	C16–C20	1.197	C9–C6	1.382
C65–C66	0.976	C80–C79	1.198	C5–C4	1.384
C186–C94	0.977	C13–C12	1.199	C79–C78	1.389
C125–C122	0.977	C30–C31	1.202	C20–C18	1.389
C212–C211	0.978	C97–C95	1.204	C145–C144	1.389
C193–C53	0.979	C100–C97	1.207	C17–C16	1.390
C33–C36	0.979	C50–C49	1.209	C178–C176	1.393
C165–C145	0.980	C155–C154	1.212	C96–C50	1.394
C196–C194	0.980	C98–C95	1.213	C173–C170	1.395
C90–C87	0.981	C17–C21	1.215	C34–C39	1.397
C214–C144	0.981	C126–C125	1.216	C153–C151	1.401
C124–C123	0.981	C7–C12	1.217	C74–C72	1.405
C1–C3	0.981	C76–C75	1.219	C101–C100	1.409
C108–C112	0.983	C21–C19	1.219	C31–C41	1.411
C113–C109	0.983	C154–C151	1.219	C75–C77	1.412
C71–C37	0.984	C25–C21	1.222	N174–C172	1.413
C89–C88	0.984	C19–C18	1.227	C86–C83	1.416
C204–C103	0.984	C30–C2	1.230	C94–C49	1.420
C121–C17	0.984	C95–C94	1.231	N174–C173	1.421
C115–C117	0.984	C141–C140	1.231	C1–C32	1.430
C53–C39	0.984	C76–C80	1.232	C127–C125	1.436
C169–C165	0.984	C9–C41	1.234	C82–C81	1.451
C110–C109	0.985	C4–C10	1.234	C161–C160	1.451
C103–C101	0.985	C81–C80	1.235	C157–C156	1.455
C151–C150	0.986	C156–C153	1.237	C99–C98	1.461
C199–C75	0.986	C24–C23	1.237	C142–C143	1.467
C218–C81	0.986	C12–C11	1.238	C159–C158	1.471
C197–C196	0.987	C72–C76	1.238	C129–C126	1.475
C42–C29	0.987	C30–C29	1.240	C137–C135	1.501
C42–C26	0.987	C1–C2	1.246	O70–C56	1.810
C49–C48	0.988	C78–C77	1.250	O93–C27	1.843
C146–C164	0.988	C139–C138	1.253	O52–C36	1.859
C18–C28	0.988	C101–C99	1.254	O51–C47	1.877
C61–C65	0.989	C148–C141	1.254	O208–C92	1.877
C118–C117	0.989	C154–C158	1.255	O116–C114	1.903
C150–C147	0.989	C139–C145	1.255	O207–C187	1.911
C73–C38	0.990	C161–C155	1.265	C8–C7	1.269
C134–C131	0.990	C138–C142	1.268	C171–C214	0.990

NMR calculation of the structure models was carried out, the result of which fitted well with the experimental spectrum of the sample, as illustrated in Figs. 10 and 11.

3.2 Study on reactivity of vitrinite concentrates and inertinite concentrates

By using Dmol3 module of the Materials Studio software, the research did calculations of the structure of the SDV molecular model which had been optimized through molecular dynamics and molecular mechanics calculations, and obtained its bond order, bond length, and electronic layouts charge number. Bond order distribution of SDV is shown in Table 8.

The bond order parameters of molecular structure may determine the active sites where chemical bonds break down, thereby to infer the relations between molecular structure and its pyrolysis. According to the data in Table 8 and in combination of analyzing calculated bond length and electronic layouts number, SDI bond with order parameters smaller than one breaks down under a certain temperature. It is concluded that in SDV molecular structure, weak bridge bonds, ether bond, aliphatic side chain, hydrogenated aromatic ring, carbonyl functional groups and the distorted parts of aromatic layer are more likely to break down, producing CO, CO_2, CH_4, monocyclic aromatic hydrocarbons and aliphatic hydrocarbons with two carbon atoms, and first-level fragments with larger molecular weights. SDV releases by pyrolysis a large number of small molecular hydrocarbons, and the macromolecular structure of coal is basically destroyed. See SDV active sites and pyrolysis in Fig. 12.

Using Dmol3 module of the Materials Studio software, the research made calculations of the structure of the SDI molecular model, which has been optimized through molecular dynamics and molecular mechanics calculations, and obtained its bond order, bond length, and electronic layouts charge number. Bond order distribution of SDI can be seen in Table 9.

According to the data in Table 9, in combination of analyzing calculated bond length and electronic layouts number, SDI with bond order parameters smaller than one breaks down under a certain temperature. SDI bond breaking occurs in the location of hydrogenated aromatic ring and carbonyl functional group, producing CH_4, CO_2, bicyclic aromatics and first-level fragments with larger molecular weights. SDV and SDI vary greatly in this phase of pyrolysis. Bond breaking points of SDV are far more than that of SDI; SDV releases through pyrolysis large amounts of small molecule hydrocarbons, leading to coal macromolecular structure basically being destroyed, while SDI releases less small molecules and obtains through pyrolysis first-level fragments with larger molecular weights. See SDI active sites and the schematic representation of pyrolysis in Fig. 13.

The analysis of maceral bond order parameters demonstrates that liquefaction mechanisms for SDV and SDI are different. For SDV, it produces pyrolysis products with small molecular weights and has a high conversion rate. To improve the yield rate of its liquefaction is to quickly stabilize active free radicals and prevent the subsequent secondary pyrolysis. The whole process is subject to thermodynamics control.

For SDI, it produces pyrolysis products with large molecular weights. To improve the yield rate of its liquefaction is to increase hydrocracking activity and severity of its macromolecule products. The whole process is subject to dynamics control.

3.3 Autoclave experiment of SDV and SDI

To prove the difference of liquefaction reaction mechanisms between SDI and SDV, hydrogenation liquefaction experiments in an autoclave were conducted respectively.

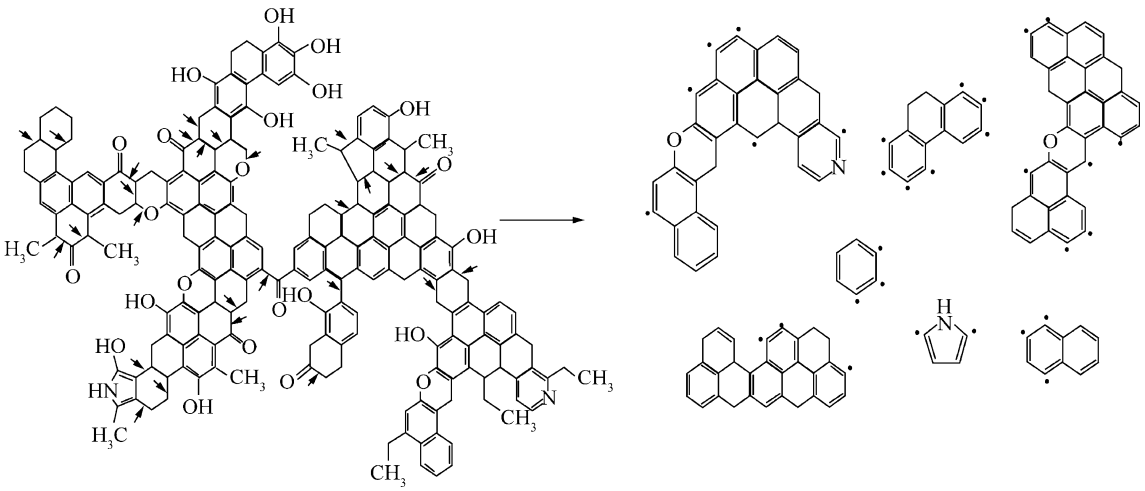

Fig. 12 Diagram on SDV active sites during the pyrolysis and the pyrolysis process

Table 9 Inertinite bond order distribution

Bond name	Bond order	Bond name	Bond order	Bond name	Bond order
O105–C97	0.922	C8–C6	1.036	C191–C189	1.287
O160–C4	0.926	C168–C130	1.038	C46–C45	1.288
C28–O221	0.932	C117–C90	1.039	C152–C150	1.288
C79–C117	0.933	O157–C52	1.051	C14–C11	1.288
C9–C8	0.942	C10–C7	1.054	C53–C52	1.288
O160–C77	0.942	C85–C98	1.077	C181–C179	1.289
C54–C22	0.953	C25–C23	1.080	C71–C69	1.295
C55–C74	0.956	C15–C14	1.081	C63–C62	1.295
C79–C78	0.956	C34–C45	1.084	C114–C112	1.298
C153–C132	0.963	C43–C27	1.089	C83–C82	1.299
C176–C174	0.965	O120–C95	1.089	C145–C152	1.299
O125–C122	0.968	C76–C60	1.089	C51–C33	1.300
C109–C108	0.968	C29–C27	1.116	C46–C48	1.301
C55–C54	0.969	C33–C31	1.118	C144–C151	1.301
O221–C68	0.969	O184–C172	1.118	C94–C102	1.304
O124–C69	0.973	C56–C24	1.132	C31–C40	1.304
C175–C174	0.975	C94–C92	1.133	C138–C123	1.306
C178–C175	0.975	C179–C177	1.134	C75–C74	1.308
O125–C61	0.976	C90–C89	1.138	C141–C139	1.309
C24–C22	0.978	O163–C161	1.146	C16–C10	1.313
C138–C154	0.979	C34–C32	1.148	C203–C202	1.314
C154–C112	0.979	C171–C181	1.149	C87–C85	1.316
C73–C70	0.979	C26–C23	1.153	C113–C112	1.321
C159–C5	0.980	C194–C191	1.156	C10–C11	1.322
C55–C57	0.981	C3–C2	1.157	C142–C141	1.323
C104–C103	0.982	C95–C93	1.157	C52–C51	1.325
C11–C9	0.982	C179–C178	1.158	C17–C14	1.325
C75–C73	0.982	C82–C115	1.158	C138–C137	1.325
C26–C44	0.984	C28–C25	1.159	C71–C70	1.326
C108–C127	0.984	C192–C189	1.165	C53–C43	1.327
C155–C153	0.985	C116–C114	1.167	C62–C60	1.335
C123–C121	0.985	C97–C96	1.167	C100–C98	1.337
C106–O105	0.986	C150–C149	1.168	C173–C3	1.337
C121–C113	0.988	C145–C144	1.169	C173–C171	1.338
C177–C176	0.989	C189–C187	1.170	C139–C75	1.342
C121–C63	0.990	C170–C180	1.176	C70–C57	1.348
O219–C213	0.990	C131–N129	1.181	C69–C68	1.349
C134–C147	0.992	C6–C3	1.183	C201–C199	1.349
C154–C153	0.994	C171–C170	1.183	C111–C113	1.350
C166–C44	0.994	C191–C190	1.191	C7–C6	1.350
C44–C158	0.996	C188–C186	1.194	C48–C47	1.351
C110–C100	0.996	C133–C144	1.194	C122–C123	1.359
C139–C126	0.996	C210–C149	1.195	C63–C61	1.359
C108–C99	0.996	C86–C84	1.197	C50–C49	1.360
C126–C64	0.996	C36–C35	1.200	C81–C80	1.361
C204–C198	0.996	C58–C66	1.201	C136–C135	1.361
C133–C132	0.997	C4–C2	1.202	C137–C136	1.363
C209–C196	0.997	C84–C82	1.212	C101–C99	1.371
C132–C116	0.997	C127–C130	1.213	C41–C39	1.374
C78–C111	0.998	C59–C58	1.213	C196–C202	1.375
C216–C215	0.999	C88–C114	1.214	C39–C38	1.380
C106–C104	0.999	C195–C193	1.214	C36–C34	1.392
C21–C20	1.000	C187–C186	1.214	C213–C210	1.393
C109–C83	1.000	C60–C58	1.214	C66–C64	1.399
C135–C161	1.001	C7–C5	1.215	C18–C17	1.401
C78–C62	1.001	C195–C194	1.216	C130–C128	1.410
C215–C48	1.002	C146–C145	1.218	C97–C95	1.410
C206–C192	1.002	C93–C101	1.219	C5–C4	1.411
C212–C137	1.002	C148–C147	1.219	C49–C47	1.411
C207–C197	1.002	C43–C35	1.219	C81–C103	1.412
C159–C76	1.003	C61–C59	1.220	C197–C203	1.413
C174–C188	1.003	O185–C181	1.220	C199–C198	1.417
C1–C87	1.004	C214–C213	1.220	C18–C16	1.418
C20–C22	1.004	C65–C64	1.227	C67–C65	1.424
C209–C176	1.004	C96–C94	1.227	C25–C24	1.430
C72–C71	1.005	C59–C67	1.231	C190–C188	1.430
C1–C110	1.006	C89–C88	1.231	C40–C38	1.431
C158–C53	1.007	C91–C86	1.233	N140–C74	1.438
C155–C151	1.007	C35–C33	1.235	C147–C133	1.450
C29–C37	1.007	C84–C88	1.236	C80–C102	1.454
C218–C214	1.008	C32–C41	1.241	C27–C26	1.454
C205–C202	1.009	C50–C45	1.244	C91–C90	1.455
C79–C77	1.010	C198–C194	1.245	C142–N140	1.455
C168–C101	1.011	C32–C31	1.248	C23–C21	1.461
C67–C72	1.011	C68–C56	1.248	C214–C211	1.463
C134–C115	1.011	C186–C196	1.249	C201–C200	1.470
C73–C65	1.011	C187–C197	1.249	C116–C115	1.484
C12–C9	1.012	C103–C96	1.249	C180–C177	1.491
C166–C30	1.012	C93–C92	1.250	C127–C131	1.493
C167–C51	1.013	C99–C98	1.250	C193–C192	1.494
C37–C36	1.013	C211–C150	1.251	C29–C28	1.500
C21–C30	1.014	C128–N129	1.254	C148–C146	1.563
C13–C12	1.016	C2–C172	1.259	O182–C178	1.576
C208–C190	1.020	C135–C122	1.265	C76–C77	1.589
C183–C180	1.021	C172–C170	1.267	C15–C13	1.768
C42–C41	1.023	C85–C83	1.270	O156–C42	1.802
C164–C152	1.029	C87–C86	1.271	O169–C168	1.812
C50–C42	1.032	C57–C56	1.273	O118–C117	1.839
O143–C141	1.034	C200–C195	1.274	O162–C161	1.847
O217–C46	1.035	C92–C100	1.275	O19–C8	1.858
O220–C210	1.035	C111–C89	1.277	O119–C54	1.945
O165–C66	1.035	C151–C149	1.285	O107–C106	1.956

Autoclave heating rate remained at 8 °C/min, and the temperature was kept constant when it reached 455 °C. The results are shown in Table 10.

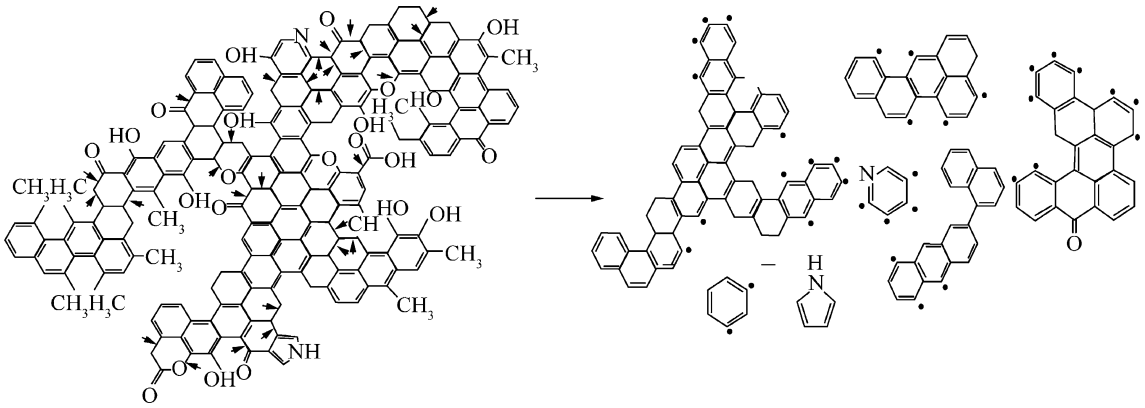

Fig. 13 Diagram on SDI active sites during the pyrolysis and the pyrolysis process

Table 10 Shenhua coal maceral liquefaction experiment results

Reaction time (min)	SDI				SDV			
	Oil yield (%)	Difference	Gas yield (%)	Difference	Oil yield (%)	Difference	Gas yield (%)	Difference
0	43.03		7.45		61.55		6.51	
30	51.32	8.29	9.51	2.06	73.16	11.61	9.01	2.50
60	58.95	7.63	10.76	1.25	74.05	0.89	12.95	3.94

As can be seen from Table 10, when it reaches the reaction temperature with a constant heating rate, i.e. the reaction time is "0", SDI oil yield (hexane solubles) is 43.03 %, rate of gasification is 7.45 %; in the same conditions, SDV oil yield goes up to 61.55 %, 18.52 % points higher than SDI, which indicates that small molecule structure are dominant in the molecular structure of SDV, and most of its pyrolysis products are small-molecule ones.

At the initial stage of the reaction, when the reaction is at its 30 min, SDI oil yield improves by 8.29 %, rate of gasification by 2.09 %; while for SDV within the same amount of time, the oil yield increases by 11.61 %, and rate of gasification is equal to that of SDI. The reason behind this is there is mainly pyrolysis happening in the initial stage of the reaction, i.e. the pyrolysis process which has not been finished in the heating process will continue in this stage. This experiment also shows that SDV is dominated by small molecule structure and its liquefaction is subject to thermodynamics control.

In the middle and late stage of the reaction, between 30 and 60 min of the reaction time, SDI oil yield improves by 7.63 %, reaching nearly 59 %, while rate of gasification increases only by 1.25 %; meanwhile, SDV oil yield increases only by 0.89 %, while rate of gasification is up 3.94 %, much higher than that of SDI.

The experiment results further demonstrate that SDI pyrolysis products have large molecular weights; the way to improve the yield rate of its liquefaction is therefore to increase the hydrocracking activity and severity of its macromolecule products. SDI liquefaction process is subject to dynamics control. On the other hand, SDV pyrolysis products have small molecular weights; the target products will have secondary pyrolysis and rate of gasification increases as reaction time and severity increases.

3.4 Efficient directional direct coal liquefaction technology fit for the macerals characteristics of Shenhua coal

Through bond order parameter analysis of molecular structure of SDV and SDI and with results of autoclave hydrogenation liquefaction experiment, the research has proved that liquefaction mechanisms of SDV and SDI are different.

As vitrinite and inertinite have different liquefaction mechanisms, and different products come from different processes, so there will inevitably be increase of gas yield if general direct coal liquefaction process is applied to Shenhua coal, which has a high content of inertinite.

Process that suits the macerals characteristics of Shenhua coal should be as follows: For vitrinite, a shorter reaction time is appropriate; reaction mechanism is mainly pyrolysis; there must be adequate active hydrogen to prevent the condensation of radical fragments of small molecules produced by pyrolysis. As regards inertinite, it requires longer reaction time and higher severity of the reaction, and the reaction mechanism is mainly hydrocracking, hence the need for high-activity catalysts and high-activity hydrogen-donating solvents.

Table 11 Results of a comparative test on common process and Shenhua process applied on Shenhua coal

Project	Foreign process	Shenhua process
P (MPa)	19	19
T (°C)	455	455
Conversion rate (%)	89.69	91.22
Product yield (%)		
Gas generated (%)	17.89	13.11
Oil products (%)	52.56	57.42

If vitrinite and inertinite of Shenhua coal can be separated respectively and the subsequent two hydrogenation processes be set, one for vitrinite, the other for inertinite, then the problem of high rate of gasification caused by different reaction mechanisms of vitrinite and inertinite can be properly addressed. But it is industrially impossible.

Process that suits the maceral characteristics of Shenhua coal is to control the reaction time of SDV and SDI in the same reaction system to avoid secondary pyrolysis of SDV light products.

Shenhua direct coal liquefaction process is bespoke developed on the basis of the maceral characteristics of Shenhua coal. It sets a gas–liquid separator in the upper part of the reactor, thus light oils produced from one-way pyrolysis of vitrinite can be separated in time at the top of the reactor to prevent secondary pyrolysis thanks to short one-way reaction time of forced circulation reactor. Macromolecule fragments produced from inertinite pyrolysis will again be put into the reactor by circulating pump for catalytic hydrogenation in order to obtain more liquid products. The whole process realized efficient, directional, and effective conversion of the vitrinite and inertinite of Shenhua coal.

Under the same reaction conditions, the research conducted a comparative test on Shenhua coal with a small 0.12 t/d direct coal liquefaction continuous unit (BSU). The results are shown in Table 11, and the data of which clearly demonstrates that gas yield of Shenhua process is significantly lower than that of foreign process as Shenhua process avoids the secondary pyrolysis of generated oil, hence a significantly higher oil yield compared to that of foreign process; meanwhile, Shenhua process extends the reaction time of heavy oil and bitumen whilst avoiding the secondary pyrolysis of generated oil, so the conversion rate of Shenhua process is higher than that of foreign process.

4 Conclusions

(1) From the constructed SDV and SDI molecular structure models, it can be seen that SDV is largely made of small molecules, while SDI is made of macromolecules.

(2) According to data about SDV and SDI molecular model bond order, bond length and electronic layouts number, they are significantly different during pyrolysis, bond breaking points of SDV are far more than that of SDI; SDV releases through pyrolysis large amounts of small molecule hydrocarbons with its macromolecular structure basically being destroyed, while SDI doesn't release through pyrolysis so much small molecules as fragments with larger molecular weights.

(3) Findings of the autoclave experiment show that SDI pyrolysis products have large molecular weights. The way to improve the yield of its liquefaction is to increase hydrocracking activity and severity of its macromolecule products. SDI liquefaction process is subject to dynamics control. Since the molecular weights of SDV pyrolysis products are relatively small, the target products will have secondary pyrolysis as reaction time and severity increases, leading to a consequent increase in gas yield. Vitrinite liquefaction can be categorized as the process of thermodynamics control.

(4) Shenhua direct coal liquefaction process that is developed on the basis of the maceral characteristics of Shenhua coal can effectively reduce its gas yield and improve oil yield.

Acknowledgments Supported by the National Engineering Laboratory of Direct Coal Liquefaction (MZY-16).

References

Lin HL, Li KJ, Zhang XW, Li YL (2013a) Study on Shendong Shangwan coal and the structure characteristics of its maceral concentrates. Coal Convers 36(2):1–5

Lin HL, Li KJ, Zhang XW (2013b) Structural characteristics and model constructing of inertinite concentrates of Shangwan coal. J Fuel Chem Technol 41(6):641–648

Shu GP (2009) History and significance of the development of Shenhua coal direct liquefaction process. Shenhua Sci Technol 27(1):78–82

Shu GP, Xu ZG (1997) Direct coal liquefaction technology. Chin Coal 10:21–24

Shu GP, Shi ShD, Li KJ (2003) Coal liquefaction technology. Coal Industry Press, Beijing, pp 97–98